Crystal structure, valence state of cations and elemental composition of manganite $Pr_{1-x}Bi_xMnO_{3+\sigma}$ according to X-ray diffraction and X-ray photoelectron spectroscopy

© K.A. Googlev[1], A.T. Kozakov[2], A.G. Kochur[1], A.V. Nikolskiy[2], A.G. Rudskaya[3]

[1] Rostov State Transport University,
Rostov-on-Don, Russia
[2] Scientific-Research Institute of Southern Federal University,
Rostov-on-Don, Russia
[3] Southern Federal University,
Rostov-on-Don, Russia

E-mail: googlev@rambler.ru

According to X-ray photoelectron spectroscopy, the ratio of the fractions of trivalent and tetravalent manganese, Mn^{3+}/Mn^{4+}, in ceramic manganite $Pr_{1-x}Bi_xMnO_{3+\sigma}$ was determined. The profiles of the X-ray photoelectron Pr4d- and Mn2p-spectra were calculated in the isolated ion approximation considering multiplet splitting in the final state of photoionization, and good agreement with the experiment was achieved.

Keywords: manganite, X-ray photoelectron spectroscopy, valence state, multiplet splitting, X-ray diffraction.

1. Introduction

Manganites with the perovskite structure $RMnO_3$, where R are rare earth elements such as La, Pr and Nd are actively studied at present due to the expected prospects of usage of their electrical and magnetic properties for creation of various solid-state electronics devices [1,2]. The initial interest in these compounds was attributable to the discovery of a giant magnetoresistance effect in them [3,4]. Subsequently, a number of interesting magnetic and electrical effects were discovered in them, in particular, the presence of positive and negative temperature coefficient of resistance [5], metal-dielectric transitions [6], ferromagnetic-paramagnetic transitions [7], and charge ordering [8]. These properties make manganites promising for their use in magnetic sensors [9], supercapacitors [10] and infrared bolometers [11,12].

The properties of manganites $RMnO_3$ that are interesting for applied studies can be modified by partial replacement of elements in the position A of the perovskite structure with other elements [13], replacement of Pr atoms with Bi atoms in our case. Such compounds can be represented by the general formula $Pr_{1-x}Bi_xMnO_3$. By changing the parameter x from 0 to 1 it is possible to obtain substances from $PrMnO_3$ to $BiMnO_3$ with different magnetic ordering of the spin magnetic moments of Mp^{3+} ions from the antifferomagnetic in the case of $PrMnO_3$ [14] to ferromagnetic ordering in $BiMnO_3$ [15]. In a more general case of the compounds with a general formula $A_{1-x}B_xMnO_3$ (where A is a rare earth ion La, Pr, Nb) the partial substitution of a rare earth element with a divalent ion ($B = $ Ca, Sr, Ba) results in the occurrence of a mixed valence state of Mn^{3+}/Mn^{4+} cations in these systems, which is an important factor according to existing theories [16–18] that determines the ratio of ferromagnetic and antiferromagnetic moments in a broad range of values x, contributions to coherent reflections, electrical resistance and values of Curie and Neel temperatures. The physical reason for the appearance of Mn^{4+} ions was explained for these compounds by the necessity to ensure the electroneutrality of the samples. The crystal structure and magnetic properties of manganites $La_{1-x}Bi_xMnO_3$ are discussed in detail in a number of papers, in particular [19,20], which could be explained only when taking into account the presence of Mn^{4+} ions, although it is not formally necessary to assume the presence of tetravalent manganese ions in such compounds for maintaining electroneutrality (since both ions, La^{3+} and Bi^{3+}, are trivalent). The need for a reliable determination of the ratio of Mn^{3+}/Mn^{4+} in mixed manganites required the development of special techniques when using X-ray spectroscopy [21] and X-ray photoelectron spectroscopy [22–24]. The fractions of trivalent and tetravalent manganese were determined in Ref. [23] for ceramic samples of $La_{1-\alpha}Bi_\beta Mn_{1+\delta}O_{3\pm\gamma}$, and in Ref. [24] for single crystals of $La_{1-x-y}Bi_xA_yMn_\alpha O_{3\pm\beta}$ ($A = $ Ba, Pb) by X-ray photoelectron spectroscopy which significantly clarified the situation with the occurrence of tetravalent manganese in formally neutral samples.

The X-ray photoelectron spectroscopy method is used in this study to determine the ratio of Mn^{3+}/Mn^{4+} in compounds $Pr_{1-x}Bi_xMnO_3$. We measured X-ray photoelectron spectra of Bi4f, Mn2p, Pr4d, O1s and C1s inner levels for this purpose. Pr4d and Mn2p are calculated in isolated ion approximation with accounting for the multiplet splitting in

the final state of photoionization. The charge state of ions in manganite $Pr_{1-x}Bi_xMnO_3$ was studied using experimental and theoretical data. The fractions of Mn^{3+} and Mn^{4+} ions were quantified.

2. Experiment

2.1. Samples preparation

The sample of $Pr_{1-x}Bi_xMnO_3$ containing 30 mol% bismuth oxide was prepared by two-stage solid-phase synthesis from a stoichiometric mixture of simple oxides Pr_2O_3 (high purity), Bi_2O_3 (pure) and MnO_2 (high purity). Tetravalent manganese oxide MnO_2 was used to create an additional oxidizing atmosphere during synthesis since it transforms into trivalent manganese oxide Mn_2O_3 at a temperature of $T = 530-540°C$ with the release of oxygen.

The initial oxides were ground in an agate mortar for 1 h for homogenization of the charge with the addition of ethyl alcohol. The charge was then dried at a temperature of $T = 400°C$ until complete drying. Tablets with a diameter of 10 mm and a height of 1.5 mm were pressed from the dried charge under a pressure of 4.9 MPa for synthesis in an air atmosphere at a temperature of $T_1 = 900°C$ for 2 h in a muffle furnace. The structure formation process was controlled by X-ray diffraction analysis. Next, the samples were repeatedly ground in an agate mortar for 1 h with the addition of ethyl alcohol, the charge was dried at $T = 400°C$ until complete drying. Then tablets with a diameter of 10 and a height of 1.5 mm were pressed at a pressure of 6.9 MPa for sintering in an air atmosphere at a temperature of $T_2 = 1100°C$ for 3 h. The rate of heating of the samples to the synthesis temperature and sintering temperature was 10 grad/min. After synthesis and sintering, the samples were cooled with the furnace to room temperature. Temperature was controlled using high-precision temperature controller VRT-3 with an accuracy of $±0.5°C$.

2.2. X-ray diffraction data

X-ray diffraction analysis of the samples was performed using the Bragg–Brentano scheme with diffractometer DRON-3M (CuK_α-radiation, Ni filter) and computer recording of X-ray diffraction profiles in the range of $20 \leq 2\theta \leq 60°$ with step-by-step detector scanning (step $\Delta(2\theta) = 0.02°$, pulse time 1 s). This interval of angles 2θ was selected because it includes the most intense diffraction peaks. The extension of the interval towards the angles of $2\theta \geq 60°$ and $2\theta \leq 20°$ provides the possibility for taking into account not only of $Pr_{1-x}Bi_xMnO_3$ phases for determination of weak peaks of higher orders of reflections but also possible impurity phases. At the same time a strong overlapping of these peaks is observed which, of course, does not improve results of the refinement of structural parameters. The acquired diffraction patterns were processed by the method of full-profile analysis using the free Powder Cell software [25] and the international
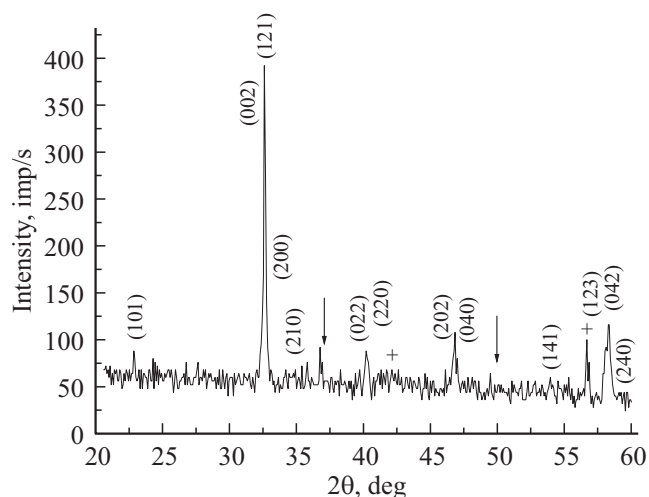

Figure 1. Fragment of a diffraction pattern of a ceramic sample of $Pr_{1-x}Bi_xMnO_3$ at room temperature. The Miller indices are specified for the orthorhombic *Pnma*-structure. The symbols ($\downarrow$) and ($+$) indicate the most intense X-ray diffraction reflections of impurity phases of Mn_2O_3 and Pr_2O_3 respectively.

crystallographic databases PDWin 3.0, and Inorganic Crystal Structure Database (ICSD).

A fragment of the diffraction pattern of a ceramic sample $Pr_{1-x}Bi_xMnO_3$ at room temperature is shown in Figure 1. It can be seen that the X-ray diffraction pattern shows peaks of impurity phases corresponding to a small amount (up to 5%) of the oxides Mn_2O_3 and Pr_2O_3 in addition to the Bragg peaks characteristic of the perovskite type structure. Impurity phases occurred after repeated annealing at $T_2 = 1100°C$, apparently as a result of partial decomposition of the solid solution at high temperature

The analysis of the splitting of the main reflections of the perovskite structure, including $(110)_C$ ($2\theta = 32.2-32.4°$), $(111)_C$ ($2\theta = 40.1-40.4°$) and $(200)_C$ ($2\theta = 46.8-47.0°$) for copper radiation with a wavelength of $\lambda = 1.54178$ Å showed that the ceramic sample of $Pr_{1-x}Bi_xMnO_3$ is characterized by an orthorhombic *Pnma* phase with cell parameters and volume at room temperature equal to $a_O = 5.472$, $b_O = 7.718$, $c_O = 5.495$ Å and $V = 232.08$ Å^3 (number of formula units $Z = 4$); in this case, the ratio of the parameters $b_O/\sqrt{2} < a_O < c_O$ is satisfied. The respective reduced perovskite subcell, per one formula unit of ABMnO$_3$ is characterized by monoclinic distortion with cell parameters $a_p = c_p = 3.878$, $b_p = 3.859$ Å, $\beta_p = 90.259°$ and $V_p = 58.02$ Å^3. The parameters and volume of a monoclinic perovskite subcell are calculated using the following formulas

$$a_p = c_p = \frac{\sqrt{a_O^2 + c_O^2}}{2}; \quad b_p = \frac{b_O}{2};$$

$$\beta_p = 2\arccos\frac{a_O}{2a_p}; \quad V_p = \frac{a_O b_O c_O}{4}. \quad (1)$$

Table 1 shows the structural parameters of $Pr_{1-x}Bi_xMnO_3$: the parameters of lattice cells ($a_O; b_O, c_O$),

Table 1. Structural parameters of $Pr_{1-x}Bi_xMnO_3$ at room temperature

| Parameter	$Pr_{1-x}Bi_xMnO_3$
a_O, b_O, c_O, Å	5.472, 7.718, 5.495
V, Å^3	232.08
Pr/Bi: $x; y; z$	0.455, 0.25, 0.513
B(Pr/Bi), Å^2	1.0
Mn: $x; y; z$	0, 0, 0.5
B(Mn), Å^2	0.1
O1: $x; y; z$	0.095, 0.25, 0.440
B(O1), Å^2	1.4
O2: $x; y; z$	0.208, 0.063, 0.778
B(O2), Å^2	0.5
R_p, %	7.61
$a_p = c_p, b_p$, Å	3.878, 3.859
β_p, $^\circ$	90.25
V_p, Å^3	58.02

positional (x, y, z) and isotropic parameters of the Debye–Waller factor (B), the profile factor of unreliability of structures (R_p) and parameters corresponding to the parameters (a_p, b_p, c_p, β_p) of monoclinic perovskite subcells. The parameters were determined with the following accuracy: for the structural parameters of the orthorhombic cell $\Delta a_O = \Delta c_O = \pm 0.003$ Å, $\Delta b_O = \pm 0.004$ Å; for cell volumes $\Delta V = \pm 0.02$ Å^3; for parameters of Debye-Waller factor $\Delta B = \pm 0.2$ Å^2; for atomic coordinates $\Delta(x/a; y/b; z/c) = \pm 0.001$, atomic coordinates are given in cell fractions; for the parameters of perovskite subcells $\Delta a_p = \Delta b_p = \Delta c_p = \pm 0.002$ Å, $\Delta \beta_p = 0.02^\circ$, $\Delta V_p = \pm 0.02$ Å^3.

For the atoms of type A, x and z in the space group $Pnma$ (№ 62) are free (adjustable) parameters: A (Pr/Bi) — $4c(x; 1/4; z)$. Mn atoms are in fixed positions: Mn — $4b(0; 0; 1/2)$, oxygen atoms O1 and O2 occupy positions $4c(x; 1/4; z)$ and $8d(x; y; z)$, respectively.

2.3. X-ray photoelectron spectroscopy data

X-ray photoelectron spectra were recorded from the surface of three samples: $Pr_{1-x}Bi_xMnO_3$ sample with an unknown ratio of Mn^{3+}/Mn^{4+}, powder of high purity Mn_2O_3 — with trivalent manganese, and ceramic sample of $SrMn^{+4}O_3$ containing tetravalent manganese. The last two samples were studied for obtaining experimental profiles of Mn2p-spectra of compounds containing only Mn^{3+} ions or only Mn^{4+} ions.

The surface of the studied ceramic samples was prepared for X-ray photoelectron measurements by mechanical scraping with a diamond scraper at a pressure of 10^{-6} Pa in the analyzer preparation chamber. The spectra of Mn2p, Pr4d, Bi4f, O1s and C1s internal levels were obtained using monochromatized X-ray radiation AlKα with an energy of 1486.6 eV and a surface analysis system with X-ray microprobe ESCALAB 250. The size of the X-ray spot
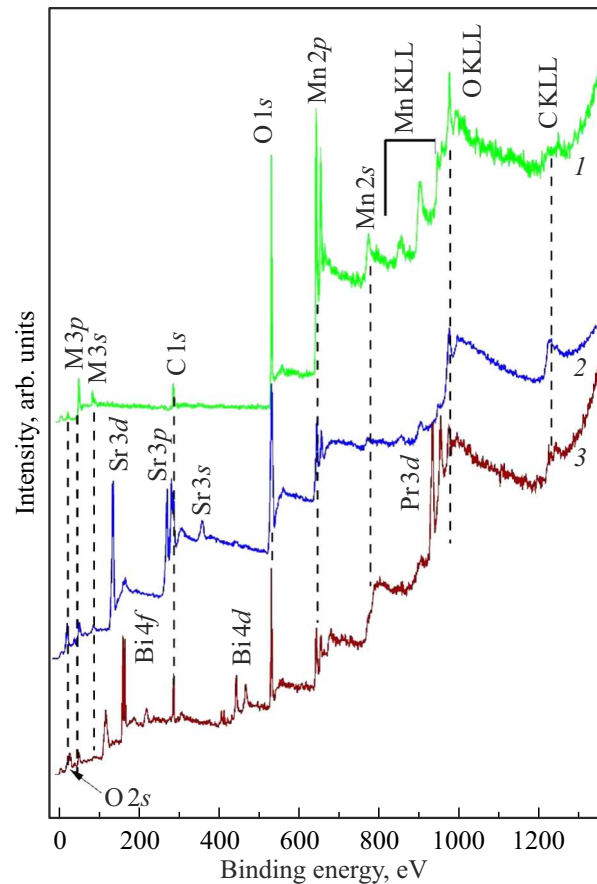
Figure 2. Survey X-ray photoelectron spectra from samples: *1* — Mn_2O_3; *2* — $SrMnO_3$; *3* — $Pr_{1-x}Bi_xMnO_3$.

on the sample surface was 500 μm. The spectra were acquired in increments of 0.1 eV. The positive charge of the sample was neutralized during spectral measurements by additional irradiation of the sample surface with a flow of slow electrons. The bond binding scales of the XPS spectra were calibrated using the carbon C1s line, the binding energy of which was was taken to be 285 eV.

Figure 2 shows the survey X-ray photoelectron spectra: *1* — from the powder of high purity Mn_2O_3; *2* — from the ceramic sample of $SrMnO_3$; *3* — from the ceramic sample of $Pr_{1-x}Bi_xMnO_3$. The analysis of the survey spectra shows that the studied samples contain only the elements which are contained in the chemical formulas of the samples, i.e. only manganese and oxygen in Mn_2O_3, strontium lines additionally appear in the survey spectrum of in $SrMnO_3$, and praseodymium and bismuth lines appear in the spectrum of $Pr_{1-x}Bi_xMnO_3$. There is a thin film of carbon on the surface of all samples, which is a surface contamination. This film is quite thin judging by the good contrast of the lines of manganese, bismuth and praseodymium.

The elemental composition of the samples was determined based on the intensities of the corresponding X-ray photoelectronic lines Mn2p, Bi4f, Pr4d and O1s using the ESCALAB 250 system software. The concentrations

of the elements were calculated using the standard approach [26,27], in which the element concentrations are determined using the relation

$$C_i(\text{at\%}) = \frac{I_i/(I_i^\infty T(E_i))}{\Sigma_j I_j/(I_j^\infty T(E_j))} \times 100\%. \qquad (2)$$

Here I_i the integral intensities of the analytical lines of the XPS, and I_i^∞ are the empirically obtained atomic sensitivity coefficients for the XPS [28], $T \sim E_{\text{kin}}^{-1/2}$ is the hardware coefficient which takes into account the dependence of the transmittance coefficient of the energy analyzer on the electron kinetic energy [27,28]. The background was cut off using the Shirley method [26].

Figure 3, a, b, d, e, shows measured X-ray photoelectron spectra of the sample of $Pr_{1-x}Bi_xMnO_3$; Figure 3, c shows Mn2p-spectrum of Mn^{3+} ion in the Mn_2O_3 sample, Figure 3, f shows Mn2p-spectrum of Mn^{4+} ion in the $SrMn^{4+}O_3$ sample.

Mn2p-spectra of all studied compounds shown in Figure 3 have two main peaks, Mn2$p_{3/2}$ and Mn2$p_{1/2}$, separated by an energy gap of ~ 11.7 eV attributable to spin-orbit splitting of the 2p-level. Mn2$p_{3/2}$-peaks of the X-ray photoelectron spectra in Figure 3, e, c and f have markedly different profiles, especially in the peak summit parts. The full widths at half maximum (FWHM) of Mn2$p_{3/2}$-peaks are also different and amount to 4.2 eV in the case of the spectrum of $Pr_{1-x}Bi_xMnO_3$, to 3.1 eV in case of the spectrum of Mn_2O_3 and to 2.5 eV in case of the spectrum of $SrMn^{+4}O_3$. Therefore, it is possible to assume that Mn2$p_{3/2}$-peak of the spectrum of $Pr_{1-x}Bi_xMnO_3$ reflects the mixed valence state of Mn^{3+}/Mn^{4+} ions of manganese [23,24,29]. The ratios of Mn^{3+}/Mn^{4+} will be determined below in Section 3 from the known profiles of M2p-spectra of Mn^{3+} and Mn^{4+} ions in accordance with the methodology provided in Refs. [23,30].

Figure 3, b shows the X-ray photoelectron spectra of the O1s levels after background subtraction. It is apparent that the O1s spectrum of oxygen has three energy components, A — 529.1 eV, B — 530.5 eV and C — 532.5 eV. The component A with a binding energy of 529.1 eV is attributed to oxygen in the crystal lattice of the studied compound. The components B and C with binding energies of 530.9 and 532.5 eV belong to the adsorbed oxygen or OH groups, respectively.

The spectrum of the Bi4f level in Figure 3, d is a doublet consisting of two peaks Bi4$f_{7/2}$ and Bi4$f_{5/2}$ separated by an energy interval of 5.3 eV attributable to the spin-orbit splitting of the 4f level. The more intense line of Bi4$f_{7/2}$ has a binding energy of 158.5 eV, and the less intense peak of Bi4$f_{5/2}$ has a binding energy of 163.8 eV. Such binding energy values are characteristic of the binding of bismuth with oxygen in the crystal lattice and correspond to the Bi ion in the trivalent state [27]. Pr4d spectrum constitutes a single peak with a bond energy of 115.3 eV, whose profile is determined by two multiplets corresponding to the main and sattelite state of Pr^{+3} ion [29].

The elemental composition determined using method (2) corresponds to the formula $Pr_{0.2}Bi_{0.541}Mn_{0.335}O_{3.923}$, which indicates an excess of oxygen on the scribed surface of the sample. The excess oxygen is represented by components B and C in Figure 3. The elemental composition of the sample will be determined more precisely in section 3 in the discussion of the experimental results using the known ratio of Mn^{3+}/Mn^{4+} according to the methodology provided in Refs. [31,32], excluding the contribution of surface oxygen.

3. Theory

3.1. Mn2p-spectra

The method of calculation of Mn2p spectra is described in detail in Refs. [23,30]. The isolated ion approximation is used in the calculations. Multiplet structures in the ion configurations of the final photoionization states of $2p^53d^4$ (Mn^{3+} ion) and $2p^53d^3$ (Mn^{4+} ion) and the corresponding ionization cross sections are calculated in the intermediate coupling approximation. The radial parts of the atomic orbitals are calculated in the corresponding ion configurations in the Pauli–Fock approximation. The integrals of the electrostatic interaction and the spin-orbit interaction constants are scaled for the best matching of the calculated spectra of Mn^{3+} and Mn^{4+} ions with the experimental spectra of $Mn_2^{+}O_3$ and $SrMn^{4+}O_3$ compounds.

The temperature sensitivity is the specific feature of Mn2p spectra which is attributable to the fact that the terms of the initial photoionization states of $2p^63d^4$ (^5D_J) and $2p^63d^4$ (^4F_J) are split by the spin-orbit interaction of electrons in the 3d-subshell. At the same time, the energy distances between the lowest J-components of these terms are small, and they can be populated by thermal excitations even at room temperature. On this basis, the spectra are calculated as superpositions of spectra

$$2p^63d^n(^{2S+1}L_J) \to 2p^53d^n + e^- \qquad (3)$$

with weights equal to the Boltzmann populations of the J-components of the terms of the initial states. The temperature dependence of the electronic spectra of 3d-metals is discussed in detail in [33,34].

Figure 4 shows the experimental Mn2p-spectra of $Mn_2^{+}O_3$ and $SrMn^{4+}O_3$ and theoretical Mn2p-spectra of Mn^{3+} and Mn^{4+} ions. The vertical bars are proportional to the calculated photoionization cross sections in the states of the multiplets $2p^53d^4$ (Mn^{3+}) and $2p^53d^3$ (Mn^{4+}). For calculation of the spectral profiles each component is replaced by a pseudo-Voigt (0.5 L+0.5 G) profile with an area equal to the photoionization cross section and a full width at half maximum of 1.5 eV.

The comparison of experimental and theoretical Mn2p spectra in Figure 4 demonstrates their good agreement suggesting the adequacy of the theoretical approaches used. It also follows from Figure 4 that the profiles of Mn2p spectra of Mn^{3+} and Mn^{4+} ions are asymmetric like the profile of Mn2p spectrum of $Pr_{1-x}Bi_xMnO_3$ compound in

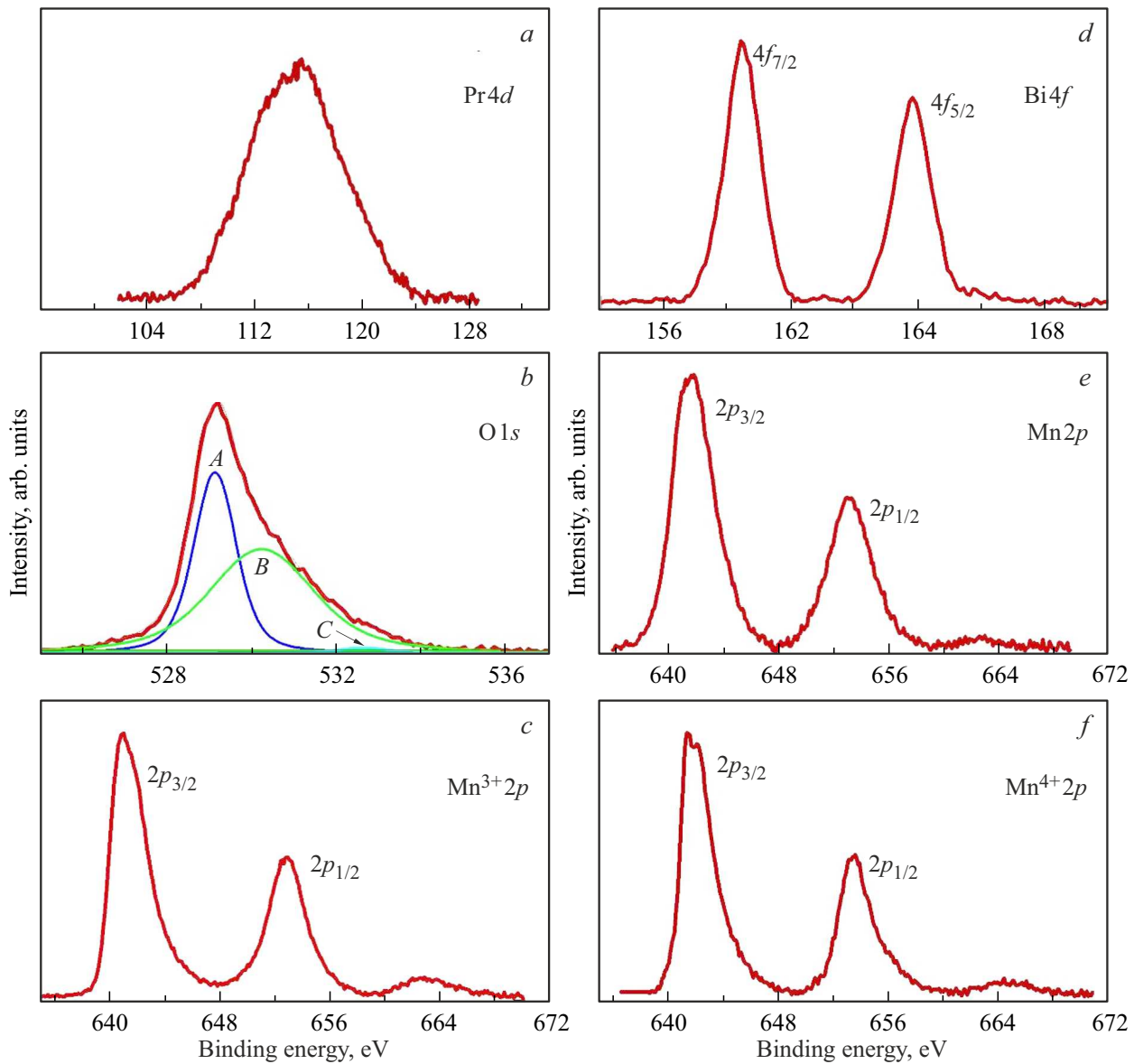**Figure 3.** a, b, d, e — Pr4d, Bi4f, O1s, Mn2p X-ray photoelectron spectra of the $Pr_{1-x}Bi_xMnO_3$ sample respectively; c — Mn2p spectrum of Mn^{3+} ion in Mn$_2$O$_3$; f — Mn2p spectrum of Mn^{4+} ion in SrMn^{4+}O$_3$.

Figure 3, e. For this reason, it seems methodically correct to determine the fractions of Mn^{3+} and Mn^{4+} ions in the compound by fitting the profile of Mn2p spectra of manganites simultaneously containing Mn^{3+} and Mn^{4+} ions not with symmetric curves (Lorentz, Gauss, or Voigt functions) [5,12], but with actual spectra of ions, either calculated [23,24,29] or experimental [31]. We will use the profiles of experimental Mn2p spectra of Mn^{3+} and Mn^{4+} ions in Mn$_2$O$_3$ and SrMnO$_3$ compounds for fitting in this study.

3.2. Pr4d-spectra

The presence of charge transfer satellites is a specific feature of Pr4d-spectra. Satellite lines along with the

„main" components of the spectra of Pr^{3+} ions reflecting the states of $4d^94f^2$ appear in the spectra reflecting states with charge transfer from ligand (L) to metal $4d^94f^3L^{-1}$. Pr4d spectrum were calculated as superpositions of the following spectra on the assumption that intramultiplet interactions prevail over intermultiplet interactions [29,35]:

$$\text{Spct}(\text{Pr4}d) = \alpha\text{Spct}(4d^{10}4f^2 \rightarrow 4d^94f^2 + \text{e}^-)$$
$$+ \beta\text{Spct}(4d^{10}4f^2 \rightarrow 4d^94f^3 + \text{e}^-). \quad (4)$$

The coefficients α and β are found by fitting (4) to the experimental spectrum. The Pr4d spectrum according to approximation (4) is an overlap of spectra with the final states Pr4d^94f^2 and Pr4d^94f^3 and charge transfer states of $4d^94f^3$ are visible due to the admixture of the states of
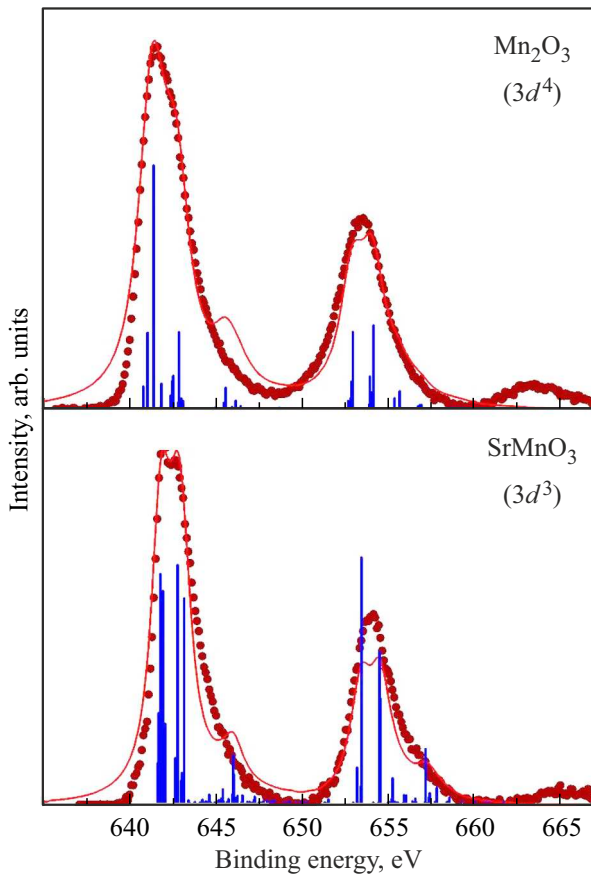
Figure 4. Theoretical spectra of Mn^{3+} ions and Mn^{4+} ions (vertical columns and solid line) and experimental spectra of $Mn_2^{3+}O_3$ and $SrMn^{4+}O_3$ compounds.

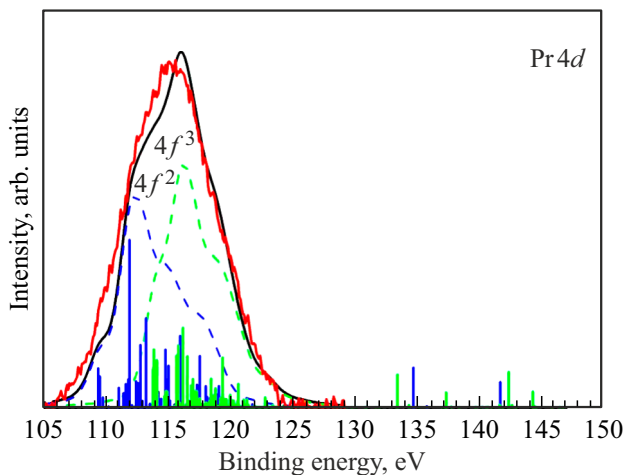**Figure 5.** Pr4d-X-ray photoelectron spectrum of the $Pr_{1-x}Bi_xMnO_3$. sample

$4d^94f^2$. A more detailed description of calculations of Pr4d spectra is provided in Ref. [29].

Figure 5 shows Pr4d photoelectron spectrum calculated using the method described above, which we use to interpret the valence state of the praseodymium.

The solid line in Figure 5 shows the result of fitting of the superposition of the spectra (4) to the experimental spectrum. The contributions of the configurations of d^94f^2 and d^94f^3 are shown by the dashed lines. It can be seen that the calculation based on the approach used is in good agreement with the experiment. It is also in good agreement with the theory [35]. Thus, it is possible to conclude that the praseodymium is in the state of Pr^{3+}.

4. Discussion

The possibility of determination of the relative fractions of Mn^{3+} and Mn^{4+} ions in practice is based on the fact that the energy positions and the profiles of the main $Mn3d_{3/2}$ peak of $Mn2p$ spectra of Mn^{3+} and Mn^{4+} ions significantly differ due to the different local charge on the manganese ions and different nature of multiplet splitting.

Figure 3, e shows the experimental spectrum of the $Mn2p$ level for $Pr_{1-x}Bi_xMnO_3$ compound. Figure 6 shows that its profile can be reproduced as a superposition of the experimental spectra off Mn_2O_3 (Mn^{3+}) and $SrMnO_3$ (Mn^{4+}) respectively.

The decomposition of the experimental $Mn2p$-spectrum presented in Figure 6 shows that manganese ions in $Pr_{1-x}Bi_xMnO_3$ compound have tri- and tetravalent states and the shares of Mn^{4+} and Mn^{3+} ions are 0.32 and 0.68, respectively. The element composition can be determined more accurately excluding surface oxygen based on the known shares of Mn^{3+} and Mn^{4+} ions in $Pr_{1-x}Bi_xMnO_3$ compound.

The following procedure was used to determine atomic concentrations taking into account the presence of several components in the intensity of the analytical of O1s line in Figure 3, b. A series of element concentrations are

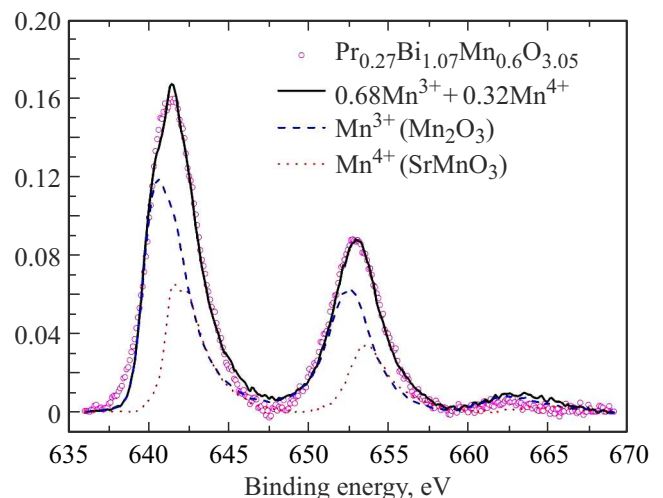**Figure 6.** Experimental $Mn2p$-spectrum of the $Pr_{1-x}Bi_xMnO_3$ sample and superposition of experimental $2p$-spectra of Mn^{3+} and Mn^{4+} ions in Mn_2O_3 and $SrMnO_3$ compounds (solid lines). The dashed and dotted lines show the contributions of Mn^{3+} and Mn^{4+} components.
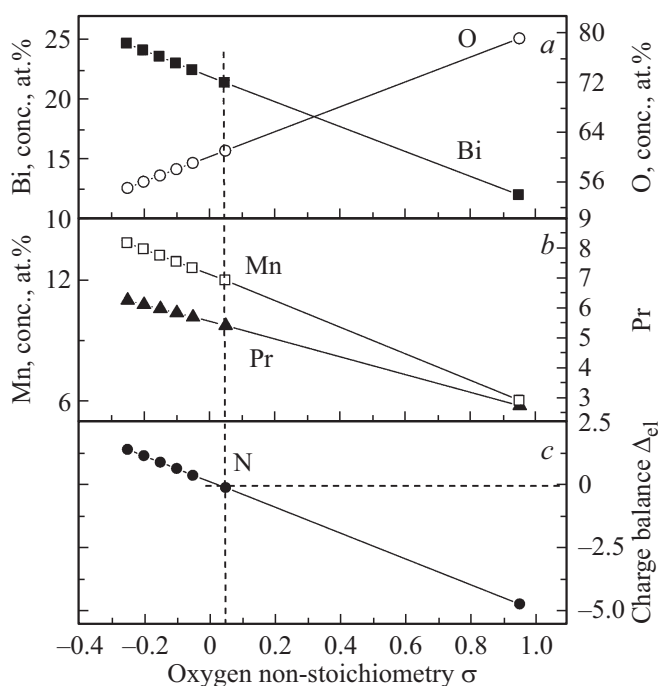
Figure 7. The concentrations of elements calculated for the Pr$_{1-x}$Bi$_x$MnO$_3$ sample with different values of the nonstoichiometry parameter for oxygen (panels *a* and *b*). The sum of the charges of all ions in the formula unit Δ_{el} (panel *c*). The concentrations of elements in the sample were determined at $\Delta_{el} = 0$. The oxygen non-nonstoichiometry for this sample is $\sigma = 0.05$.

Table 2. The concentrations of elements (in atomic percentages) and the formular composition of the sample of Pr$_{1-x}$Bi$_x$MnO$_{3+\sigma}$ obtained on the assumption of electroneutrality of the sample

Sample	Pr$_{1-x}$Bi$_x$MnO$_{3+\sigma}$			
	Pr	Bi	Mn	O
Concentration, at%	5.42	21.47	12.02	61.08
Formular composition	Pr$_{0.27}$Bi$_{1.07}$Mn$_{0.6}$O$_{3.05}$			

Aliovalent manganese ions were previously observed in case of isovalent substitution in manganites La$_{1-\alpha}$Bi$_\beta$Mn$_{1+\delta}$O$_{3\pm\gamma}$ with a bismuth molar concentration of $\beta < 0.5$ [23,34]. The presence of oxygen vacancies in the material can be one of the mechanisms of the appearance of Mn^{4+} ions. This mechanism should be excluded in the case of our Pr$_{0.27}$Bi$_{1.07}$Mn$_{0.6}$O$_{3.05}$ compound because there are no oxygen vacancies. It can be assumed that the presence of Mn^{4+} ions in the Pr$_{0.27}$Bi$_{1.07}$Mn$_{0.6}$O$_{3.05}$ sample may be due to the distortions of the crystal lattice because of different ion radii $r(\mathrm{Pr}^{3+}) = 1.11$ Å and $r(\mathrm{Bi}^{3+}) = 1.15$ Å [36–38].

5. Conclusion

Pr$_{0.27}$Bi$_{1.07}$Mn$_{0.6}$O$_{3.05}$ compound was synthesized. The lattice cell parameters were determined using X-ray diffraction method. X-ray diffraction measurements showed that the content of the main phase in the sample reaches 95%. The application of the method described in this paper for determining the element composition using X-ray photoelectron spectroscopy shows the presence of an excessive oxygen equal to $\sigma = +0.05$ in the sample of Pr$_{0.27}$Bi$_{1.07}$Mn$_{0.6}$O$_{3.05}$. The analysis of the profile of Mn2p spectrum showed the presence of tri- and tetravalent manganese ions in the sample. The shares of Mn^{3+} and Mn^{4+} ions are equal to 0.68 and 0.32.

Conflict of interest

The authors declare that they have no conflict of interest.

determined for the sample with fixed input intensities of lines of Mn2p, Bi4f, Pr4d and different intensities of the component of O1s line related to oxygen embedded in the crystal structure of the sample.

The latter, taking into account the found concentrations of manganese, made it possible to calculate separately the concentrations of Mn^{3+} and Mn^{4+} ions and their shares in the total cationic charge of the sample. The knowledge of the atomic concentrations and ion charges made it possible to determine the charge balance Δ_{el}, i.e. the sum of the charges of all cations (Pr^{3+}, Bi^{3+}, Mn^{3+} and Mn^{4+}) and anions (O^{2-}) in the formula unit of the sample. Figure 7, *a, b* shows the dependences of element concentrations on the oxygen nonstoichiometry parameter σ for the sample of Pr$_{1-x}$Bi$_x$MnO$_3$. Panel c shows the dependence of the charge balance Δ_{el} on σ.

The element composition of the sample is determined at $\Delta_{el} = 0$ according to the methodology proposed in Refs. [31,32]. The requirement of the electroneutrality of the sample is satisfied if the value σ, corresponding to the point N on the line characterizing the dependence of Δ_{el} on σ is selected in Figure 7, *c*. A vertical straight line passing through the point N intersects with the concentration dependencies for Mn, Bi and Pr (panels *a* and *b* Figure 7); these intersection points give the desired concentrations of the elements. The ion concentrations calculated in this manner for the sample studied in this work is provided in Table 2.

References

[1] N.E. Massa, L. Campo, D.D.S. Meneses, M.J. Martínez-lope, J.A. Alonso. J. Phys. Condens. Matter **25**, 235603 (2013).

[2] Q. Renwen, L. Zhe, F. Jun. Phys. B: Condens. Matter **406**, 1312 (2011).

[3] S. Jin, T.H. Tiefel, M. McCormack, R.A. Fastnacht, R. Ramesh, L.H. Chen. Science **264**, 413 (1994).

[4] H. Wang, H. Zhang, K. Su, S. Huang, W. Tan, D. Huo. J. Mater. Sci. Mater. Electron. **31**, 14421 (2020).

[5] J. Han, X. Yu, Sh. Jin, X. Guan, X. Gu, Y. Yan, K. Wu, L. Zhao, J. Jiang, J. Peng, H. Liu, X. Liu. Ceram. Int. **49**, 4386 (2023).

[6] T. Sun, F. Ji, Y. Liu, G. Dong, S. Zhang, Q. Chen, X. Liu. J. Eur. Ceram. Soc. **39**, 352 (2019).

[7] N. Assoudi, I. Walha, E. Dhahri, S. Alleg, E.K. Hlil. Solid State Commun. **277**, 13 (2018).

[8] J.Y. Fan, Y.F. Xie, Y.E. Yang, C.X. Kan, L.S. Ling, W. Tong, C.X. Wang, C.L. Ma, W.F. Sun, Y. Zhu, H. Yang. Ceram. Int. **45**, 9179 (2019).

[9] S.A. Yang, Q.M. Chen, Y.R. Yang, Y. Gao, R.D. Xu, H. Zhang, J. Ma. J. Alloys Compd. **882**, 160719 (2021).

[10] H.Y. Mo, H.S. Nan, X.Q. Lang, S.J. Liu, L. Qiao, X.Y. Hu, H.W. Tian. Ceram. Int. **44**, 9733 (2018).

[11] X.L. Guan, K.L. Chu, H.J. Li, X.R. Pu, X.H. Yu, S.Z. Jin, Y. Zhu, S.H. Sun, J.B. Peng, X. Liu. J. Alloys Compd. **876**, 160173 (2021).

[12] X. Pu, H. Li, G. Dong, K. Chu, S. Zhang, Y. Liu, X. Yu, X. Liu. Ceram. Int. **46**, 4984 (2020).

[13] E. Hernández, V. Sagredo, G.E. Delgado. Rev. Mex. Fis. **61**, 166 (2015).

[14] B. Dabrowskia, S. Kolesnika, A. Baszczukb, O. Chmaissema, T. Maxwella, J. Mais. J. Solid State Chem. **178**, 629 (2005).

[15] A. Moreira dos Santos, A.K. Cheetham, T. Atou, Y. Syono, Y. Yamaguchi, K. Ohoyama, H. Chiba. Phys. Rev. B **66**, 064425 (2002).

[16] E.O. Wollan, W.C. Koehler. Phys. Rev. **100**, *2*, 545 (1955).

[17] J.B. Goodenough. Phys. Rev. **100**, *2*, 564 (1955).

[18] E. Dagotto, T. Hotta, A. Moreo. Phys. Rep. **344**, 1 (2001).

[19] I.O. Troyanchuk, O.S. Mantytskaja, H. Szymczak, M.Yu. Shvedun. Low Temp. Phys. **28**, *7*, 569 (2002).

[20] V.A. Khomchenko, I.O. Troyanchuk, O.S. Mantytskaya. ZhETF **130**, *1* (*7*), 64 (2006). (in Russian).

[21] V.R. Galakhov, M.C. Falub, K. Kuepper, M. Neumann. J. Struct. Chem. **49**, Supplement S54 (2008).

[22] V.R. Galakhov, M. Demeter, S. Bartkowski, M. Neumann, N.A. Ovechkina, E.Z. Kurmaev, N.I. Lobachevskaya, Ya.M. Mukovskii, J. Mitchell, D.L. Ederer. Phys. Rev. B **65**, 113102 (2002).

[23] A.G. Kochur, A.T. Kozakov, A.V. Nikolskii, K.A. Googlev, A.V. Pavlenko, I.A. Verbenko, L.A. Reznichenko, T.I. Krasnenko. J. Electron Spectrosc. Rel. Phenom. **185**, 175 (2012).

[24] A.T. Kozakov, A.G. Kochur, L.A. Reznichenko, L.A. Shilkina, A.V. Pavlenko, A.V. Nikolskii, K.A. Googlev, V.G. Smotrakov. J. Electron Spectrosc. Rel. Phenom. **186**, 14 (2013).

[25] W. Kraus, G. Nolze. J. Appl. Cryst. **29**, 301 (1996).

[26] Practical Surface Analysis by Auge rand X-Ray Photoelectron Spectroscopy / Eds D. Briggs, M.P. Seach. John Wiley & Sons, Chichester (1983). 533 p.

[27] V.I. Nefedov. Rentgenovskaya fotoelektronnaya spektroskopiya khimicheskikh soedineniy. Khimiya, M. (1984). P. 256. (in Russian).

[28] Handbook of X-Ray Photoelectron Spectroscopy / Eds C.D. Wagner, W.M. Riggs, L.E. Davis, J.F. Moulder. Perkin-Elmer Corporation, Eden Prairie, Minnesota, USA (1979). 190 p.

[29] A.T. Kozakov, A.G. Kochur, V.G. Trotsenko, A.V. Nikolskii, M. El Marssi, B.P. Gorshunov, V.I. Torgashev. J. Alloys Compd. **740**, 132 (2018).

[30] A.T. Kozakov, A.G. Kochur, A.V. Nicolsky, K.A. Googlev, V.G. Smotrakov, V.V. Eremkin. J. Electron Spectrosc. Rel. Phenom. **184**, 508 (2011).

[31] N.A. Liedienov, Z. Wei, V.M. Kalita, A.V. Pashchenko, Q. Li, I.V. Fesych, V.A. Turchenko, C. Hou, X. Wei, B. Liu, A.T. Kozakov, G.G. Levchenko. Appl. Mater. Today. **26**, 101340 (2022).

[32] A.T. Kozakov, A.G. Kochur, A.V. Nikolskii, I.P. Raevski, S.P. Kubrin, S.I. Raevskaya, V.V. Titov, A.A. Gusev, V.P. Isupov, G. Lid, I.N. Zakharchenko. J. Electron Spectrosc. Rel. Phenom. **239**, 146918 (2020).

[33] A.G. Kochur, A.T. Kozakov, V.A. Yavna, Ph. Daniel. J. Electron Spectrosc. Rel. Phenom. **195**, 200 (2014).

[34] A.G. Kochur, A.T. Kozakov, K.A. Googlev, A.V. Nikolskii. J. Electron Spectrosc. Rel. Phenom. **195**, 1 (2014).

[35] H. Ogasawara, A. Kotani, R. Potze, G.A. Sawatzky, B.T. Thole. Phys. Rev. B **44**, 5465 (1991).

[36] P. Orgiani, A. Galdi, C. Aruta, V. Cataudella, G. De Filippis, C.A. Perroni, V. Marigliano Ramaglia, R. Ciancio, N.B. Brookes, M. Moretti Sala, G. Ghiringhelli, L. Maritato. Phys. Rev. B **82**, *20*, 205122 (2010).

[37] P. Orgiani, C. Aruta, R. Ciancio, A. Galdi L. Maritato. J. Nanoparticle Res. **15**, 1655 (2013).

[38] R.D. Shannon. Acta crystallogr. A: Cryst. Phys. Diffr. Theor. Gen. Crystallogr. **32**, *5*, 751 (1976).

Translated by A.Akhtyamov